www.sciencemag.org/cgi/content/full/340/6133/724/DC1

Supplementary Materials for

Spin-Optical Metamaterial Route to Spin-Controlled Photonics

Nir Shitrit, Igor Yulevich, Elhanan Maguid, Dror Ozeri, Dekel Veksler, Vladimir Kleiner, Erez Hasman*

*Corresponding author. E-mail: mehasman@technion.ac.il

Published 10 May 2013, *Science* **340**, 724 (2013)

This PDF file includes:

Materials and Methods

Sample preparation

The artificial kagome structures were formed on a SiC-6H single polytype crystal substrate using advanced photolithographic techniques. A NiCr film was deposited on the substrate and overcoated with a positive photoresist. After exposing the photoresist through a mask, it was developed leaving a pattern on the NiCr film. A Cr etchant was then applied to remove the NiCr film from the exposed areas. At this point the photoresist was removed and the substrate was etched by a reactive ion etching (RIE) through the NiCr voids serving as a mask. The RIE was performed at a power of 250 W and a pressure of 40 mTorr with CF_4 and O_2 gas flow rates of 13.8 and 1.2 sccm, respectively. The etching performed at a rate of 35 Å/min at the room temperature was continued until the desired depth was reached. As a final step, the remaining NiCr was removed with a Cr etchant.

Polarization analysis

The Stokes parameters are a set of values representing the polarization state of electromagnetic radiation determined by measuring the intensity of the radiative field through a polarizer and a retarder (*29*). In the experiment, we used a circular polarizer, i.e., a quarter-wave plate followed by a linear polarizer in different orientations (see Fig. S1). Let α be the quarter-wave plate orientation and β be the polarizer transmission axis orientation, the intensity can be calculated using the Mueller matrix as

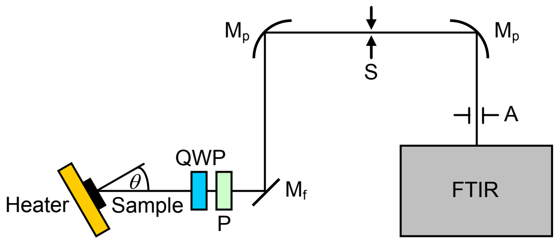

Fig. S1. Experimental measurement setup. Angle-resolved thermal emission spectra at varying polar angle θ are measured by a Fourier transform infrared (FTIR) spectrometer. The radiation polarization state is analyzed using a circular polarizer (a quarter-wave plate (QWP) followed by a linear polarizer (P)), and then guided by a flat mirror (M_f) and parabolic mirrors (M_p) with a focal length of 250 mm, via an angular resolution slit (S) in the focal plane of M_p and a field of view aperture (A).

$$\begin{aligned} I(\alpha,\beta) &= \frac{S_0}{2} + \\ &\frac{S_1}{2}\cos 2\alpha(\cos 2\alpha \cos 2\beta + \sin 2\alpha \sin 2\beta) + \\ &\frac{S_2}{2}\sin 2\alpha(\cos 2\alpha \cos 2\beta + \sin 2\alpha \sin 2\beta) + \\ &\frac{S_3}{2}(\sin 2\alpha \cos 2\beta - \cos 2\alpha \sin 2\beta). \end{aligned} \tag{1}$$

The intensities were captured for the combinations of $(\alpha,\beta) = (0°,0°)$, $(45°,0°)$, $(-45°,0°)$, and $(45°,45°)$. With these four measurements, we calculated the Stokes parameters as a function of the different intensities to be

$$\begin{aligned} S_0 &= I(45°,0°) + I(-45°,0°), \\ S_1 &= 2I(0°,0°) - S_0, \\ S_2 &= 2I(45°,45°) - S_0, \\ S_3 &= I(45°,0°) - I(-45°,0°). \end{aligned} \tag{2}$$

Experimental measurement setup

Angle-resolved thermal emission spectra were measured by mirror optics (Fig S1). The sample was heated to $773 \pm 1\mathrm{K}$, where the temperature was measured with K-type thermocouple and controlled by a temperature controller (HeatWave Labs 101303-04). The measurements of the emission spectra, in the range of polar angles θ from $-50°$ to $50°$, were performed using a FTIR spectrometer (Bruker-Vertex 70) equipped with a cooled HgCdTe detector. The spectral resolution was set to $1\mathrm{cm}^{-1}$, the field of view was chosen as 8 mm to avoid edge effects (each sample is 12 mm square), and the angular resolution was selected as $0.1°$.

Supplementary Text

Isotropic kagome lattice

In addition to the artificial anisotropic kagome lattice (KL) structures, a KL with isotropic antennas was also realized. The isotropic KL consists of circular voids with a nearest-antenna distance of 6.5 μm (see Fig. S2A). Such an isotropic metamaterial, which is inversion symmetric (IS) in all directions (i.e., the inversion transformation $\mathbf{r} \to -\mathbf{r}$ preserves the structure), resembles the $q = 0$ configuration and serves as a reference for the investigation of the structural lattice. Angle-resolved thermal emission spectra were measured by a FTIR spectrometer at varying polar and fixed azimuthal angles (θ, φ), respectively, while heating the sample to 773 K (see Fig. 1C for the experimental setup). The dispersion relations $\omega(k)$ at $\varphi = 60°$ and $90°$ of the isotropic KL structure are shown in Fig. S2, B and C, respectively, and exhibits a good agreement with the standard momentum-matching calculation $\mathbf{k}_\mathbf{e}^{\parallel} = \mathbf{k}_{\mathbf{SPP}} + m\mathbf{G}_1 + n\mathbf{G}_2$. Here, $\mathbf{k}_\mathbf{e}^{\parallel}$ is the wavevector of the emitted light in the surface

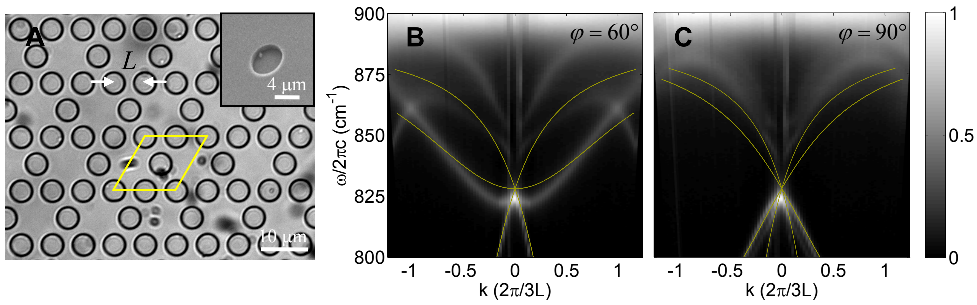

Fig. S2. (**A**) Optical microscope image of the isotropic KL. The rhombus represents the unit cell in the real space. The inset is a scanning electron microscope image of the circular antenna, with a diameter of 4.8 μm, 1 μm etched upon a SiC substrate. (**B** and **C**) Measured intensity dispersions of thermal emission from the isotropic KL structure along the directions of $\varphi = 60^\circ$ and 90°, respectively. The lines correspond to the standard momentum-matching calculation.

plane, $\mathbf{k}_{\mathbf{SPP}}$ is the surface phonon polariton (SPP) wavevector, (m,n) are the indices of the radiative modes, and $(\mathbf{G}_1,\mathbf{G}_2)=\frac{\pi}{L}\left(\mathbf{x}+\frac{\mathbf{y}}{\sqrt{3}},-\mathbf{x}+\frac{\mathbf{y}}{\sqrt{3}}\right)$ are the lattice reciprocal vectors.

Local field distribution in spinoptical metamaterials

The observed Rashba spin splitting in the $\sqrt{3}\times\sqrt{3}$ kagome two-dimensional (2D) lattice is twice the one detected in the 2D square lattice with space-variant antennas along a specific direction (*22*, *23*); this peculiarity lies in the geometric nature of the vertex-sharing triangles. In contrast to the one-dimensional (1D) rotation rate, the local field distribution in the KL is highly affected by the coupled nearest-neighbor antennas restricted by the triangular symmetry (Fig. S3B) and not by the straight line (Fig. S3A). Specifically, the phase accumulation of 2π along an inversion

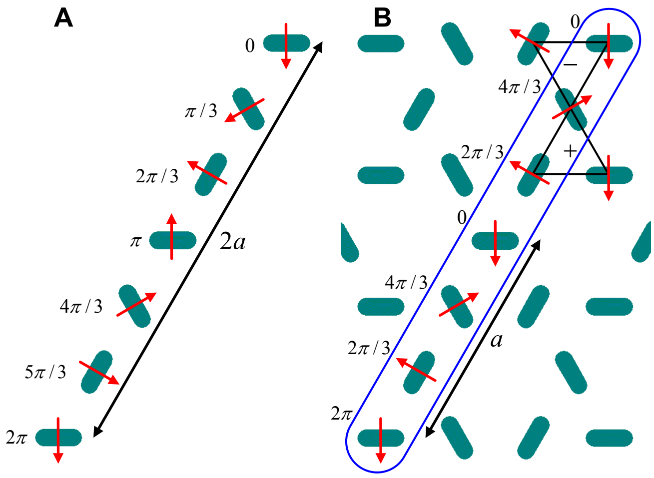

Fig. S3. (**A**) The field periodicity of a 1D spinoptical metamaterial represented by the identical phases – arrows – is $2a$, where a is the structural periodicity. (**B**) The field periodicity of the 2D staggered chirality kagomé metamaterial is a. The chirality is denoted by the sign inside the triangle and it is positive when the arrows rotate by $+120°$ as traversing anticlockwise around a triangle, and vice versa.

asymmetric (IaS) direction in the $\sqrt{3}\times\sqrt{3}$ kagome is obtained along the half distance attained in the 1D geometric gradient structure. In general, the shift corresponds to the field periodicity; in the latter, the field periodicity is twice the structural one, whereas, in the former, these periodicities are identical. Hence, the Rashba dispersion spin splitting in the staggered chirality kagome structure is $\Delta k = 2\pi / a$, where $a = 3L$ is the rotation period and L is the nearest-antenna distance, while in the array with 1D inhomogeneity rate it is π / a.

Optical Rashba effect

In the Rashba effect, owing to the spin-orbit interaction under broken inversion symmetry, the spin-degenerate parabolic bands split into dispersions with oppositely spin-polarized states, whose energy values are denoted by $E^{\pm}(\mathbf{k}) = \hbar^2\mathbf{k}^2/2m^* \pm \alpha_R|\mathbf{k}|$ (*18-21*). Here, $\mathbf{k}$ is the electron momentum, m^* is the effective mass of electrons, and α_R is the Rashba parameter representing the strength of the Rashba effect. The Rashba dispersion prescribes the momentum Rashba offset of $\Delta k_R \propto \alpha_R$ and the accompanied Rashba energy splitting of $E_R \propto \alpha_R^2$.

In order to study the optical Rashba effect, we follow a specific parabola-like mode, governed by the spin-orbit momentum-matching (SOMM) condition $\mathbf{k}_\mathbf{e}^{\parallel}(\sigma) = \mathbf{k}_\mathbf{SPP} + m\mathbf{G}_\mathbf{1} + n\mathbf{G}_\mathbf{2} - \sigma\mathbf{K}_\mathbf{i}$, when φ varies (see Fig. S4A); here, $\sigma_\pm = \pm 1$ is the optical spin corresponding to right- and left-circularly polarized light, respectively, and $i \in \{1,2\}$ is the index of the specific spin-dependent geometric Rashba term from the orientational reciprocal vectors $\mathbf{K}_{\mathbf{1},\mathbf{2}} = \frac{\pi}{3L}\left(-\mathbf{x} \mp \sqrt{3}\mathbf{y}\right)$. For the σ_- solution with the indices $(m,n) = (0,-1)$ and $i = 1$, we yield the relation $\omega^2 = a_1\Delta k_R^2 + a_2\cos(\varphi + 60°)\Delta k_R + a_3$, where Δk_R is the Rashba splitting and (a_1, a_2, a_3) are constants. In analogy to the Rashba effect, the normalized optical Rashba energy is defined as the frequency differences between the minima of the parabolic bands at an IS direction and some φ, i.e., $\Delta\omega_R = \omega_{IS} - \omega(\varphi)$. Since $\Delta\omega_R << \omega_{IS}$ one can obtain the relation between the optical Rashba energy and the Rashba splitting via $\Delta\omega_R = b_1\Delta k_R^2 + b_2\cos(\varphi + 60°)\Delta k_R + b_3$ with the constants (b_1, b_2, b_3). By utilizing the SOMM condition, we calculated $\Delta k_R(\varphi)$ and yielded the linear relation $\Delta k_R \propto \cos(\varphi + 60°)$ (Fig. S4B); hence, the optical Rashba energy-momentum splitting relation takes the well-known electronic Rashba form $\Delta\omega_R = c_1\Delta k_R^2 + c_2$ with the corresponding (c_1, c_2) constants (Fig. S4C). In this manner,

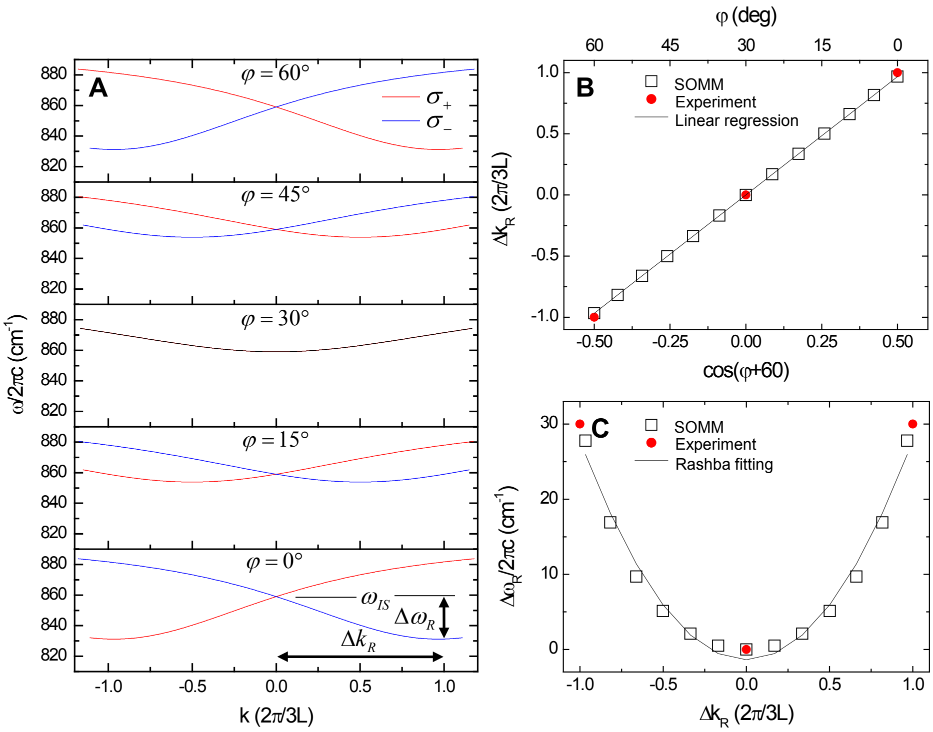

Fig. S4. (**A**) The dynamics of the spin-dependent modes as the direction traverses from IaS to IS to IaS. The red and blue parabola-like modes correspond to $\sigma_{\pm}$ solutions with the indices $(m,n,i)=(0,\pm1,1)$. In the IS direction the modes are spin-degenerated as shown by the black line. The Rashba splitting and the normalized optical Rashba energy are denoted by Δk_R and $\Delta\omega_R$, respectively; note that the crossing between the modes at $k=0$ is obtained at a constant frequency which is ω_{IS}. (**B**) The Rashba splitting exhibits a linear dependence on the $\cos(\varphi+60°)$ parameter. (**C**) The normalized optical Rashba energy obeys the Rashba energy-momentum splitting relation depicted by the parabolic fitting.

the SOMM is a generalized condition since it validates the fundamental Rashba splittings.

This analysis sheds light on the spin-polarized dispersion of the $\sqrt{3}\times\sqrt{3}$ structure at varying φ. Specifically, the resulting condition of $\Delta\omega_R \propto \cos^2(\varphi+60°)$ brings a physical insight for the maximal and minimal Rashba energies associated with the IaS and IS directions, respectively (see Fig. 3, A and B).

Momentum-matching condition from symmetry analysis

Let $\boldsymbol{\psi}(\mathbf{r},t)$ be a vector function. Note that if we transform the coordinates by a translation $\mathbf{r'}=T\mathbf{r}$, the transformation that $\boldsymbol{\psi}$ undergoes is $\hat{T}\boldsymbol{\psi}=\boldsymbol{\psi}(T^{-1}\mathbf{r},t)$; if we transform the coordinates by a rotation (or mirroring) $\mathbf{r'}=R\mathbf{r}$ then $\boldsymbol{\psi}$ will transform as $\hat{R}\boldsymbol{\psi}=R\boldsymbol{\psi}(R^{-1}\mathbf{r},t)$ (*33*). These actions define a group representation of coordinate transformations on the functions space.

Consider two transformations of the Cartesian coordinate system $\mathbf{r}=\begin{pmatrix} x \\ y \end{pmatrix}$: (i) a shift to the left $T\mathbf{r}=\mathbf{r}-\mathbf{s}$, where $\mathbf{s}=\begin{pmatrix} 2L \\ 0 \end{pmatrix}$ (see Fig. S5B), and (ii) a rotation of $120°$ anticlockwise by the matrix R of $\begin{pmatrix} -1/2 & -\sqrt{3}/2 \\ \sqrt{3}/2 & -1/2 \end{pmatrix}$ around the axis depicted in Fig. S5A. One can see that the $\sqrt{3}\times\sqrt{3}$ KL is invariant to the combined transformation $\hat{U}=\hat{R}\hat{T}$ so

$$\hat{U}n(\mathbf{r})=n(T^{-1}R^{-1}\mathbf{r})=n(\mathbf{r}), \tag{3}$$

where $n(\mathbf{r})$ stands for the refractive index of the metamaterial. Moreover, the action of $\hat{R}$ and $\hat{T}$ on $n(\mathbf{r})$ commute $\hat{R}\hat{T}n(\mathbf{r})=\hat{T}\hat{R}n(\mathbf{r})=n(\mathbf{r})$.

The key observation is the following: if the wave equation is invariant with respect to the action of some group, in order for one solution $\boldsymbol{\psi}_\mathbf{i}$ to be coupled with

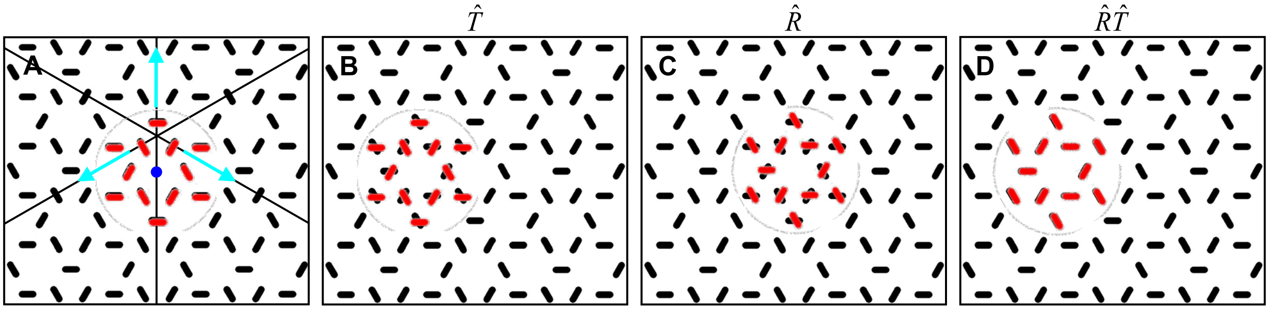

Fig. S5. (**A**) The axis of rotation in the $\sqrt{3}\times\sqrt{3}$ KL is depicted by the blue point. The lines show the mirror symmetry directions. The blue arrows represent the symmetric mode $\boldsymbol{\psi}_{\mathbf{f}}^{(1)}$ which is invariant under mirror reflection. (**B** to **D**) $\hat{T}$, $\hat{R}$, and $\hat{R}\hat{T}$ transformations of the $\sqrt{3}\times\sqrt{3}$ KL.

another solution $\boldsymbol{\psi}_{\mathbf{f}}$, both $\boldsymbol{\psi}_{\mathbf{i}}$ and $\boldsymbol{\psi}_{\mathbf{f}}$ must transform similarly under the action of the group (*34*). Let $\boldsymbol{\psi}_{\mathbf{i}} = \boldsymbol{\varepsilon} e^{i(\omega t - k_z z)}$ be a circularly polarized wave advancing along $-\mathbf{z}$ direction in free space. If we consider a circularly polarized light as a rotating in time linear polarization, a spin-dependent phase is gained when rotating the $x-y$ plane so $\hat{U}\boldsymbol{\psi}_{\mathbf{i}} = \hat{R}\boldsymbol{\psi}_{\mathbf{i}} = e^{i2\pi\sigma/3}\boldsymbol{\psi}_{\mathbf{i}}$, where $\sigma_{\pm} = \pm 1$ is the optical spin corresponding to right- and left-circularly polarized light, respectively. We are now looking for solutions traveling in the $x-y$ plane transforming as the eigenvector $\boldsymbol{\psi}_{\mathbf{i}}$. Since $\hat{R}$ commutes with $\hat{T}$, such solutions should be eigenvectors of both transformations. A general eigenfunction of $\hat{T}$ should be of the Bloch form, $\mathbf{u}_{\mathbf{k}}(\mathbf{r})e^{i(\mathbf{k}_{\mathbf{f}}\cdot\mathbf{r}-\omega t)}$, where $\mathbf{u}_{\mathbf{k}}(\mathbf{r})$ is a periodic function; for simplicity, we assume that $\mathbf{u}_{\mathbf{k}}(\mathbf{r}) \equiv 1$, where this assumption does not affect the result.

Three types of lattice modes which are eigenvectors of $\hat{R}$ can be constructed from the Bloch functions propagating in the $x-y$ plane

$$\boldsymbol{\psi}_\mathbf{f}^{(1)} = \boldsymbol{\varepsilon}'\left(e^{i\mathbf{k}_\mathbf{f}\cdot\mathbf{r}} + e^{i\mathbf{k}_\mathbf{f}\cdot R^{-1}\mathbf{r}} + e^{i\mathbf{k}_\mathbf{f}\cdot R^{-2}\mathbf{r}}\right),$$

$$\boldsymbol{\psi}_\mathbf{f}^{(2)} = \boldsymbol{\varepsilon}'\left(e^{i\mathbf{k}_\mathbf{f}\cdot\mathbf{r}} + e^{-i2\pi\sigma/3}e^{i\mathbf{k}_\mathbf{f}\cdot R^{-1}\mathbf{r}} + e^{i2\pi\sigma/3}e^{i\mathbf{k}_\mathbf{f}\cdot R^{-2}\mathbf{r}}\right), \quad (4)$$

$$\boldsymbol{\psi}_\mathbf{f}^{(3)} = \boldsymbol{\varepsilon}'\left(e^{i\mathbf{k}_\mathbf{f}\cdot\mathbf{r}} + e^{i2\pi\sigma/3}e^{i\mathbf{k}_\mathbf{f}\cdot R^{-1}\mathbf{r}} + e^{-i2\pi\sigma/3}e^{i\mathbf{k}_\mathbf{f}\cdot R^{-2}\mathbf{r}}\right),$$

where the harmonic time dependence is omitted (*35*); here, $\boldsymbol{\varepsilon}'$ is a linear polarization in the $\mathbf{z}$ direction. Moreover, the aforementioned solutions correspond to eigenvalues of 1, $e^{i2\pi\sigma/3}$ and $e^{-i2\pi\sigma/3}$, respectively. These modes will be also eigenvectors of $\hat{T}$ if the momentum $\mathbf{k}_\mathbf{f}$ satisfies the equalities

$$e^{i\mathbf{k}_\mathbf{f}\cdot\mathbf{s}} = e^{i\mathbf{k}_\mathbf{f}\cdot R^{-1}\mathbf{s}} = e^{i\mathbf{k}_\mathbf{f}\cdot R^{-2}\mathbf{s}}. \quad (5)$$

Under these conditions we obtain that $\hat{T}\boldsymbol{\psi}_\mathbf{f} = e^{i\mathbf{k}_\mathbf{f}\cdot\mathbf{s}}\boldsymbol{\psi}_\mathbf{f}$ and $\hat{U}\boldsymbol{\psi}_\mathbf{f}^{(\mathbf{j})} = \hat{R}\left(\hat{T}\boldsymbol{\psi}_\mathbf{f}^{(j)}\right) = e^{i\mathbf{k}_\mathbf{f}\cdot\mathbf{s}}\hat{R}\boldsymbol{\psi}_\mathbf{f}^{(\mathbf{j})} = e^{i\left(\mathbf{k}_\mathbf{f}\cdot\mathbf{s}+2\pi\xi^{(j)}/3\right)}\boldsymbol{\psi}_\mathbf{f}^{(\mathbf{j})}$, where $\xi^{(j)} = 0, \sigma, -\sigma$ for modes $j = 1, 2, 3$, respectively. At this point, we require that $\boldsymbol{\psi}_\mathbf{f}^{(\mathbf{j})}$ and $\boldsymbol{\psi}_\mathbf{i}$ transform similarly, meaning that the eigenvalues should be equal

$$e^{i\left(\mathbf{k}_\mathbf{f}\cdot\mathbf{s}+2\pi\xi^{(j)}/3\right)} = e^{i2\pi\sigma/3}. \quad (6)$$

When solving Eqs. (5) and (6), we obtain equation system for $\mathbf{k}_\mathbf{f}$

$$\mathbf{k}_\mathbf{f}\cdot\mathbf{s} = \mathbf{k}_\mathbf{f}\cdot R^{-1}\mathbf{s} = \mathbf{k}_\mathbf{f}\cdot R^{-2}\mathbf{s} = 2\pi\left(\sigma - \xi^{(j)}\right)/3 \mod 2\pi. \quad (7)$$

Note that one equation in this set depends on the other so the equation system is not overdetermined. Moreover, mode 2 does not yield a spin-dependent solution and can not be considered to describe the optical Rashba effect.

In order to set the possible solution from the two remained modes, we seek for an additional symmetry restriction in the investigated system. Besides to the aforementioned $\hat{U}$-invariance the symmetry group of the KL system has mirror symmetries as well. Hence $\boldsymbol{\psi}_\mathbf{i}$ and $\boldsymbol{\psi}_\mathbf{f}$ must transform similarly under mirror transformation. The circularly polarized wave $\boldsymbol{\psi}_\mathbf{i}$ transforms under a mirror transformation like a 2D representation (mirroring right-handed polarized light results in left-handed polarized light); however, the mirror reflection preserves mode $\boldsymbol{\psi}_{\mathbf{f}}^{(1)}$ (see Fig. S5A), i.e., this mode transforms as the trivial 1D representation. Since $\boldsymbol{\psi}_{\mathbf{i}}$ and $\boldsymbol{\psi}_{\mathbf{f}}^{(1)}$ does not transform similarly, the coupling between them is impossible, and we obtain only the solution of $\boldsymbol{\psi}_{\mathbf{f}}^{(3)}$.

A calculation of the equation system (7) for $\boldsymbol{\psi}_{\mathbf{f}}^{(3)}$ yields the spin-dependent solution of

$$\mathbf{k_f} = -\begin{pmatrix} \pi/3L \\ \pi/\sqrt{3}L \end{pmatrix}\sigma + \mathbf{G_{m,n}}\,, \tag{8}$$

where $\mathbf{G_{m,n}}$ is a vector of a reciprocal lattice, generated by the $q=0$ KL with the basis vectors $\begin{pmatrix} 2L \\ 0 \end{pmatrix}$ and $\begin{pmatrix} -L \\ \sqrt{3}L \end{pmatrix}$. Note that the spin-dependent vector is the specific geometric Rashba correction associated with the local field distribution in the $\sqrt{3}\times\sqrt{3}$ KL. This momentum selection rule obviously governs the spontaneous emission from a structure supporting surface wave, such that the momentum-matching condition

$$\mathbf{k_e^{\parallel}} = \mathbf{k_{SPP}} - \begin{pmatrix} \pi/3L \\ \pi/\sqrt{3}L \end{pmatrix}\sigma + \mathbf{G_{m,n}} \tag{9}$$

still holds, where $\mathbf{k_e^{\parallel}}$ is the wavevector of the emitted light in the surface plane and $\mathbf{k_{SPP}}$ is the SPP wavevector.

Spin symmetry breaking in the near-field of a spinoptical metamaterial

The reciprocity between the near- and far-fields manifests that the spin-split dispersion of the emitted light is a signature of a symmetry breaking in the near-field;

therefore, we were motivated to investigate the electromagnetic fields distribution in the vicinity of the $\sqrt{3}\times\sqrt{3}$ surface. One can find in the artificial staggered chirality KL three building blocks – "geometric metamolecules" – consisting of differently oriented anisotropic nanoantennas (see Fig. S6G insets). The electromagnetic near-field distribution was calculated by a finite difference time domain (FDTD) algorithm (RSoft FullWAVE). The $\sqrt{3}\times\sqrt{3}$ kagome structure consisting of 1×2.7 μm^2 rectangular voids, imbedded to a depth of 1 μm into a SiC substrate, with a nearest distance of 6.5 μm, was normally illuminated with circularly polarized light at a wavelength of 12 μm. The normal E_z fields for incident spins of $\sigma_\pm$ were detected at 0.5 μm above the SiC-air interface (Fig. S6, A and B, respectively), where a spin degeneracy removal is observed. More particularly, a chain of vortices with alternating helicities along the IaS directions is revealed (Fig. S6, C to F). These optical vortices carry an orbital angular momentum (OAM) of $l\hbar$ per photon manifested by the spiral phase of the SPPs stemming from the spin-orbit interaction, where the integer number l is the topological charge (*36*). The OAM of the "geometric metamolecules" was calculated via an overlap integral between the numerical phase distribution $e^{-i\phi(\varphi)}$ and a spiral phase $e^{-im\varphi}$, where m is an integer and φ is the azimuthal angle. Explicitly, the weighting function of the topological charge is expressed by $\gamma_m = |\lambda_m|^2$, where $\lambda_m = N\sum_{r=R_1}^{R_2}\int_0^{2\pi} e^{-im\varphi}e^{-i\phi(\varphi)}d\varphi$, $r\in\{R_1,R_2\}$ is the radius of the path and N is an area normalizing constant. The calculation presented in Fig. S6G was performed within the interval of $R_1 = 0$ and $R_2 = 2.2\,\mu\text{m}$. Local OAM of $l = \{-2,+1,+1\}$ and $\{-1,-1,+2\}$ were calculated for $\sigma_\pm$ illuminations, respectively, for the sequence of the "geometric metamolecules" in the optical lattice unit cell (Fig.

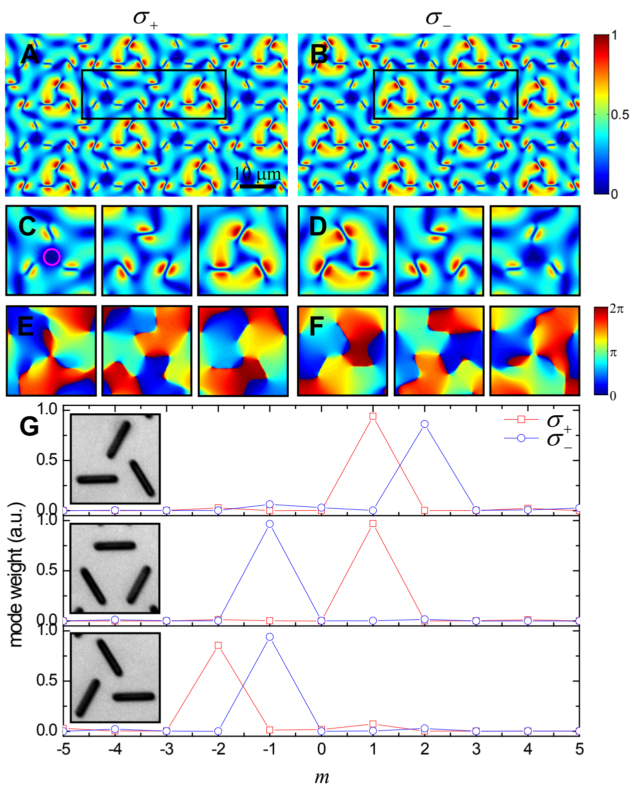

Fig. S6. (**A** and **B**) FDTD simulations of the normal E_z field amplitudes for incident spins of σ_+ (**A**) and σ_- (**B**). The rectangles show the unit cell of the three "geometric metamolecules". (**C** and **D**) Amplitude distributions of the "geometric metamolecules" sequence for σ_+ (**C**) and σ_- (**D**). (**E** and **F**) Phase distributions of the aforementioned sequence for σ_+ (**E**) and σ_- (**F**). (**G**) Local topological charge calculation of the "geometric metamolecules" for $\sigma_\pm$. The insets show optical microscope images of the "geometric metamolecules". The circle in (**C**) shows the area where this calculation was performed.

S6G). This spin-dependent space-variant OAM along the IaS directions is associated with an OAM gradient (*37*), inducing the observed spin degeneracy removal in the near-field. Therefore, the spin symmetry breaking in the near- and far-fields is a fundamental manifestation of the space-variant OAM and the Rashba geometric gradient along the IaS directions in the $\sqrt{3}\times\sqrt{3}$ KL, respectively.

References and Notes

1. R. A. Shelby, D. R. Smith, S. Schultz, Experimental verification of a negative index of refraction. *Science* **292**, 77 (2001). doi:10.1126/science.1058847

2. J. B. Pendry, Negative refraction makes a perfect lens. *Phys. Rev. Lett.* **85**, 3966 (2000). doi:10.1103/PhysRevLett.85.3966 Medline

3. W. Cai, U. K. Chettiar, A. V. Kildishev, V. M. Shalaev, Optical cloaking with metamaterials. *Nat. Photonics* **1**, 224 (2007). doi:10.1038/nphoton.2007.28

4. A. V. Rogacheva, V. A. Fedotov, A. S. Schwanecke, N. I. Zheludev, Giant gyrotropy due to electromagnetic-field coupling in a bilayered chiral structure. *Phys. Rev. Lett.* **97**, 177401 (2006). doi:10.1103/PhysRevLett.97.177401 Medline

5. S. Zhang *et al.*, Negative refractive index in chiral metamaterials. *Phys. Rev. Lett.* **102**, 023901 (2009). doi:10.1103/PhysRevLett.102.023901 Medline

6. Z. Jacob, L. V. Alekseyev, E. Narimanov, Optical hyperlens: Far-field imaging beyond the diffraction limit. *Opt. Express* **14**, 8247 (2006). doi:10.1364/OE.14.008247 Medline

7. H. N. S. Krishnamoorthy, Z. Jacob, E. Narimanov, I. Kretzschmar, V. M. Menon, Topological transitions in metamaterials. *Science* **336**, 205 (2012). doi:10.1126/science.1219171

8. V. S. Liberman, B. Y. Zel'dovich, Spin-orbit interaction of a photon in an inhomogeneous medium. *Phys. Rev. A* **46**, 5199 (1992). doi:10.1103/PhysRevA.46.5199 Medline

9. K. Y. Bliokh, Y. Gorodetski, V. Kleiner, E. Hasman, Coriolis effect in optics: Unified geometric phase and spin-Hall effect. *Phys. Rev. Lett.* **101**, 030404 (2008). doi:10.1103/PhysRevLett.101.030404 Medline

10. N. M. Litchinitser, Structured light meets structured matter. *Science* **337**, 1054 (2012). doi:10.1126/science.1226204

11. O. Hosten, P. Kwiat, Observation of the spin Hall effect of light via weak measurements. *Science* **319**, 787 (2008). doi:10.1126/science.1152697

12. Y. Gorodetski, A. Niv, V. Kleiner, E. Hasman, Observation of the spin-based plasmonic effect in nanoscale structures. *Phys. Rev. Lett.* **101**, 043903 (2008). doi:10.1103/PhysRevLett.101.043903 Medline

13. K. Y. Bliokh, A. Niv, V. Kleiner, E. Hasman, Geometrodynamics of spinning light. *Nat. Photonics* **2**, 748 (2008). doi:10.1038/nphoton.2008.229

14. N. Shitrit, I. Bretner, Y. Gorodetski, V. Kleiner, E. Hasman, Optical spin Hall effects in plasmonic chains. *Nano Lett.* **11**, 2038 (2011). doi:10.1021/nl2004835 Medline

15. M. V. Berry, The adiabatic phase and Pancharatnam's phase for polarized light. *J. Mod. Opt.* **34**, 1401 (1987). doi:10.1080/09500348714551321

16. Z. Bomzon, V. Kleiner, E. Hasman, Pancharatnam—Berry phase in space-variant polarization-state manipulations with subwavelength gratings. *Opt. Lett.* **26**, 1424 (2001). doi:10.1364/OL.26.001424 Medline

17. J. K. Gansel *et al.*, Gold helix photonic metamaterial as broadband circular polarizer. *Science* **325**, 1513 (2009). doi:10.1126/science.1177031

18. G. Dresselhaus, Spin-orbit coupling effects in zinc blende structures. *Phys. Rev.* **100**, 580 (1955). doi:10.1103/PhysRev.100.580

19. E. I. Rashba, Properties of semiconductors with an extremum loop. 1. Cyclotron and combinational resonance in a magnetic field perpendicular to the plane of the loop. *Sov. Phys. Solid State* **2**, 1109 (1960).

20. K. Ishizaka *et al.*, Giant Rashba-type spin splitting in bulk BiTeI. *Nat. Mater.* **10**, 521 (2011). doi:10.1038/nmat3051 Medline

21. P. D. C. King *et al.*, Large tunable Rashba spin splitting of a two-dimensional electron gas in Bi_2Se_3. *Phys. Rev. Lett.* **107**, 096802 (2011). doi:10.1103/PhysRevLett.107.096802 Medline

22. N. Dahan, Y. Gorodetski, K. Frischwasser, V. Kleiner, E. Hasman, Geometric doppler effect: Spin-split dispersion of thermal radiation. *Phys. Rev. Lett.* **105**, 136402 (2010). doi:10.1103/PhysRevLett.105.136402 Medline

23. K. Frischwasser, I. Yulevich, V. Kleiner, E. Hasman, Rashba-like spin degeneracy breaking in coupled thermal antenna lattices. *Opt. Express* **19**, 23475 (2011). doi:10.1364/OE.19.023475 Medline

24. See supplementary materials on *Science* Online.

25. D. Grohol *et al.*, Spin chirality on a two-dimensional frustrated lattice. *Nat. Mater.* **4**, 323 (2005). doi:10.1038/nmat1353 Medline

26. R. Moessner, A. P. Ramirez, Geometrical frustration. *Phys. Today* **59**, 24 (2006). doi:10.1063/1.2186278

27. W. Schweika, M. Valldor, P. Lemmens, Approaching the ground state of the kagomé antiferromagnet. *Phys. Rev. Lett.* **98**, 067201 (2007). doi:10.1103/PhysRevLett.98.067201 Medline

28. T. W. Ebbesen, H. J. Lezec, H. F. Ghaemi, T. Thio, P. A. Wolff, Extraordinary optical transmission through sub-wavelength hole arrays. *Nature* **391**, 667 (1998). doi:10.1038/35570

29. E. Collett, *Polarized Light: Fundamentals and Applications* (Marcel Dekker, New York, 1993).

30. N. Yu *et al.*, Light propagation with phase discontinuities: Generalized laws of reflection and refraction. *Science* **334**, 333 (2011). doi:10.1126/science.1210713

31. E. S. Barnard, R. A. Pala, M. L. Brongersma, Photocurrent mapping of near-field optical antenna resonances. *Nat. Nanotechnol.* **6**, 588 (2011). doi:10.1038/nnano.2011.131 Medline

32. A. Schiffrin *et al.*, Optical-field-induced current in dielectrics. *Nature* **493**, 70 (2013). doi:10.1038/nature11567 Medline

33. J. F. Cornwell, *Group Theory and Electronic Energy Bands in Solids* (North-Holland, Amsterdam, 1969).

34. M. S. Dresselhaus, G. Dresselhaus, A. Jorio, *Group Theory: Application to the Physics of Condensed Matter* (Springer, Berlin, 2008).

35. L. P. Bouckaert, R. Smoluchowski, E. Wigner, Theory of Brillouin zones and symmetry properties of wave functions in crystals. *Phys. Rev.* **50**, 58 (1936). doi:10.1103/PhysRev.50.58

36. L. Allen, M. W. Beijersbergen, R. J. C. Spreeuw, J. P. Woerdman, Orbital angular momentum of light and the transformation of Laguerre-Gaussian laser modes. *Phys. Rev. A* **45**, 8185 (1992). doi:10.1103/PhysRevA.45.8185 Medline

37. A. O. Santillán, K. Volke-Sepúlveda, A. Flores-Pérez, Wave fields with a periodic orbital angular momentum gradient along a single axis: A chain of vortices. *New J. Phys.* **11**, 043004 (2009). doi:10.1088/1367-2630/11/4/043004